Supporting Information

Materials. *p*-Chlorophenol and 1,4,5,8-naphthalenetetracarboxylic dianhydride were obtained from Aladdin Industrial Corporation. Ethanol, Na_2SO_4, $KMnO_4$ and ethylene diamine were all provided by the Sinopharm Chemical Reagent, China. Carbon nanotube (CNT) fibers (SCNC-F300) were provided by Suzhou Jiedi Nano Science and Technology Co., Ltd., China.

Materials characterization. The surface morphologies and structures were characterized by scanning electron microscope (SEM, Hitachi FE-SEM S-4800 operated at 1 kV) and transmission electron microscope (TEM, JEOL JEM-2100F operated at 200 KV). The energy-dispersive X-ray (EDX) elemental mappings were obtained on Bruker Xflash 6130 EDS system on a ZEISS EVO LS15 SEM set EHT at 20 KV. X-ray photoelectron spectroscopy (XPS) was recorded on an AXIS ULTRA DLD XPS System with MONO Al source (Shimadzu Corp.). Photoelectron spectrometer was recorded by using monochromatic Al KR radiation under vacuum at 5×10^{-9} Pa. All of the binding energies were referred to the C1s peak at 284.6 eV of the surface adventitious carbon. X-ray diffraction (XRD) patterns were recorded using a Bruker D8 Advance X-ray diffractometer. Raman spectra were recorded using a HORIBA JobinYvon XploRA Laser Raman spectrometer with an Ar 514.5 nm laser. Infrared spectra were recorded using a Nicolet 6700 FT-IR spectrometer. The weight of the fiber electrodes were measured by a microbalance (Sartarious SE2, resolution of 0.1 μg). The tensile strength of the fiber was tested by an HY0350 Table-top Universal Testing Instrument. Gas adsorption and pore size distribution were conducted on an automatic N_2 adsorption/desorption instrument (Micromeritics 3Flex).

Conductivity measurements. The electrical resistance was measured by a Victor VC9807A$^+$ digital multimeter. Electrical conductivity was then calculated according to the equation of $\sigma = RS/L$, where σ, R, S and L represent the electrical conductivity ($S\cdot cm^{-1}$), electrical resistance (Ω), cross-sectional area (cm^2) and length (cm), respectively.

Electrochemical Measurements. All electrochemical measurements, including the galvanostatic charge−discharge profiles, cyclic voltammograms, electrochemical impedance spectrum as well as cycling performance measurements were tested by a CHI 660a electrochemical workstation and an Arbin electrochemical station (MSTAT-5 V/10 mA/16Ch). The electrochemical performance of a single electrode (positive or negative) was characterized with three-electrode system in 1 M Na_2SO_4

electrolyte solution with a saturated calomel electrode (SCE) as the reference electrode and carbon electrode as the counter electrode. For PI/CNT fiber electrode, the electrolyte solution was purged with argon gas during the testing procedure. Electrochemical impedance spectrum was measured at frequencies ranging from 0.01 Hz to 100 KHz with a potential perturbation of 5 mV. All measurements were carried out at room temperature.

The specific capacitance (C_X) of a single fiber electrode was obtained from the charge-discharge curve based on the following equation: $C_X = It/XU$, where I, t and U are the discharge current, discharge time, and voltage window, respectively. X can be the surface area (A), volume (V) or mass (m) of the electrode. The fiber electrodes were considered to be a cylinder. Thus, the surface area (A) and volume (V) of the electrodes were determined from $A = \pi DL$ and $V = \pi D^2L/4$, where D was the diameter of the fiber and L was the length of the fiber electrode immersed into the electrolyte. If not specially declared, L was 2 cm in this work.

Electrochemical performance of the FAS was measured by two electrode method. Therefore, the areal specific capacitance ($C_{cell,A}$), volumetric specific capacitance ($C_{cell,V}$) or gravimetric specific capacitance ($C_{cell,m}$) of the entire FAS could be calculated from $C_{cell,X} = It/X_{cell}U$, where X_{cell} stands for the total surface area (A_{cell}), volume (V_{cell}) or mass (m_{cell}) of the positive and negative electrode. Correspondingly, the areal/volumetric/gravimetric energy density (E_X) and areal/volumetric/gravimetric power density (P_X) of the entire FAS could be obtained from $E_X = C_{cell,X}U^2/2$ and $P_X = E_X/t$, respectively.

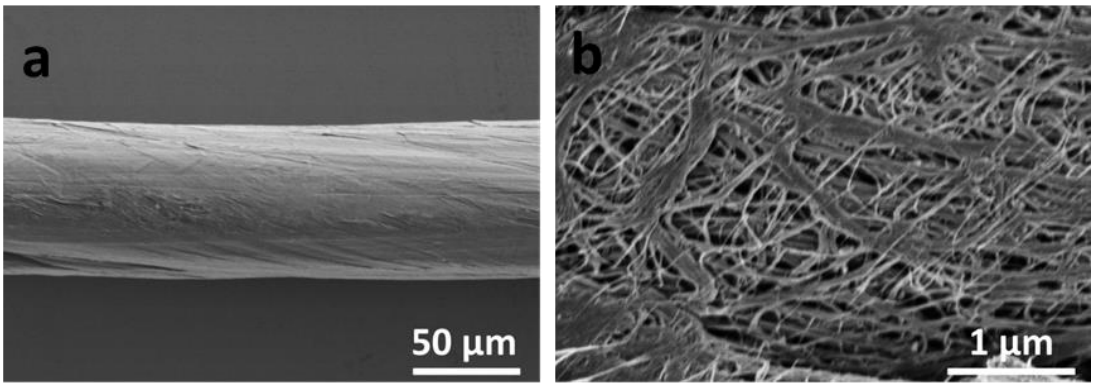

Fig. S1. (a, b) SEM images of the bare CNT fiber at increasing magnifications.

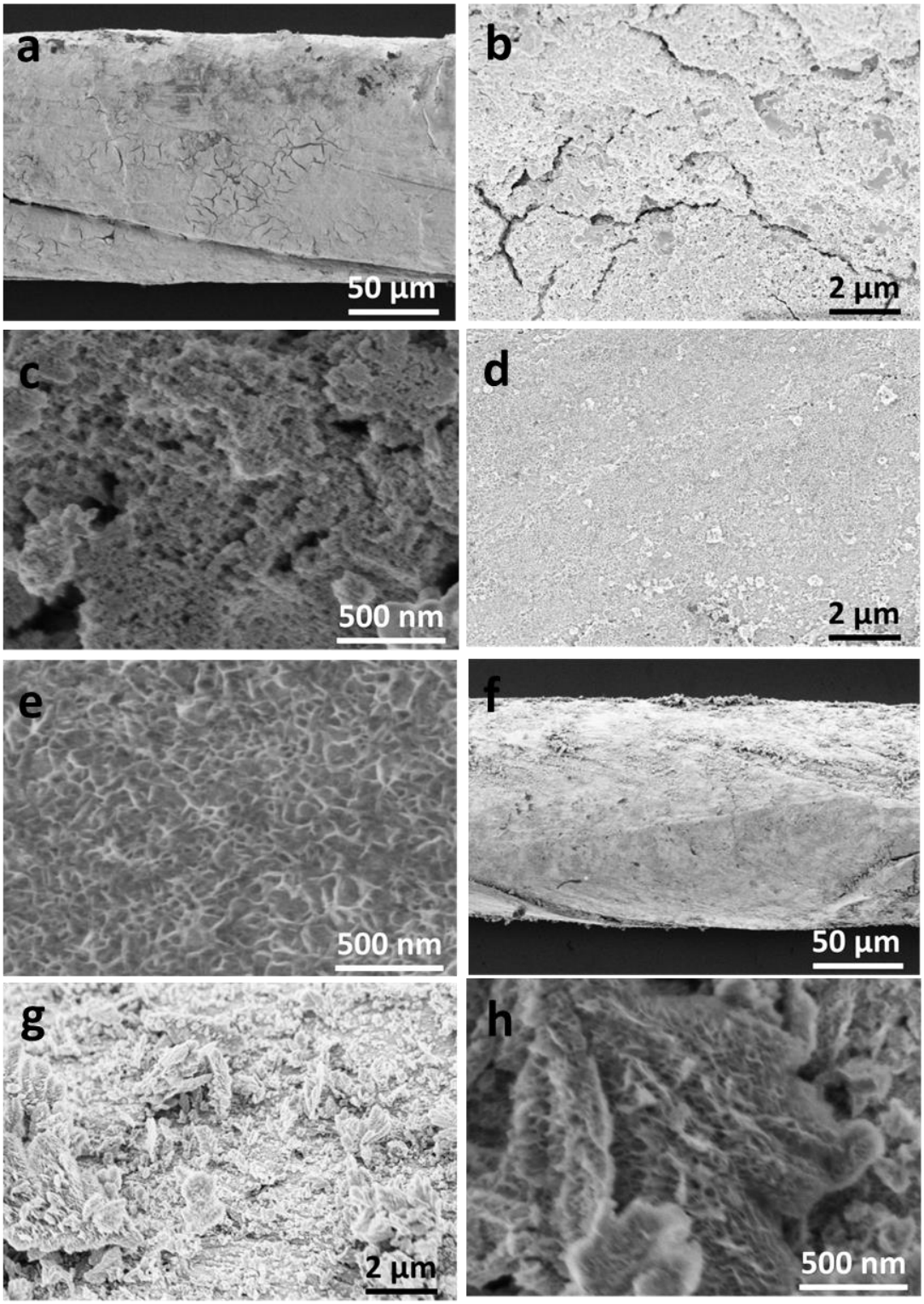

Fig. S2. SEM images of the MnO_2/CNT fibers with MnO_2 growth time of (a-c) 3 h, (d, e) 6 h and (f-h) 9 h at different magnifications.

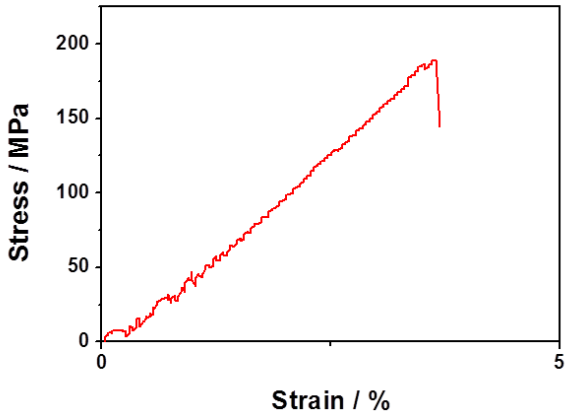

Fig. S3. Stress-strain curve of the MnO_2/CNT fiber with a MnO_2 growth time of 6 h.

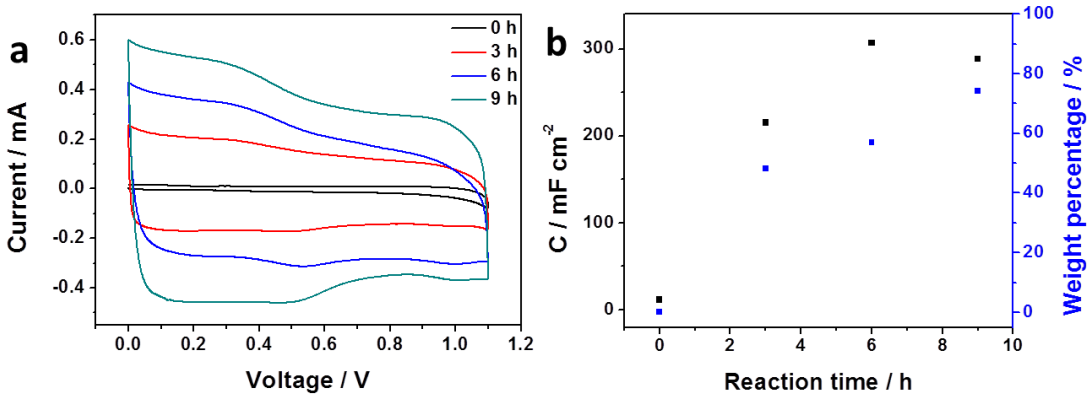

Fig. S4. (a) Comparative CV curves of MnO_2/CNT fiber electrodes with different growth times at the same scan rate of 10 $mV \cdot s^{-1}$. (b) Dependence of areal specific capacitance of MnO_2/CNT fiber and weight percentage of MnO_2 on reaction time measured at 1.91 $mA \cdot cm^{-2}$.

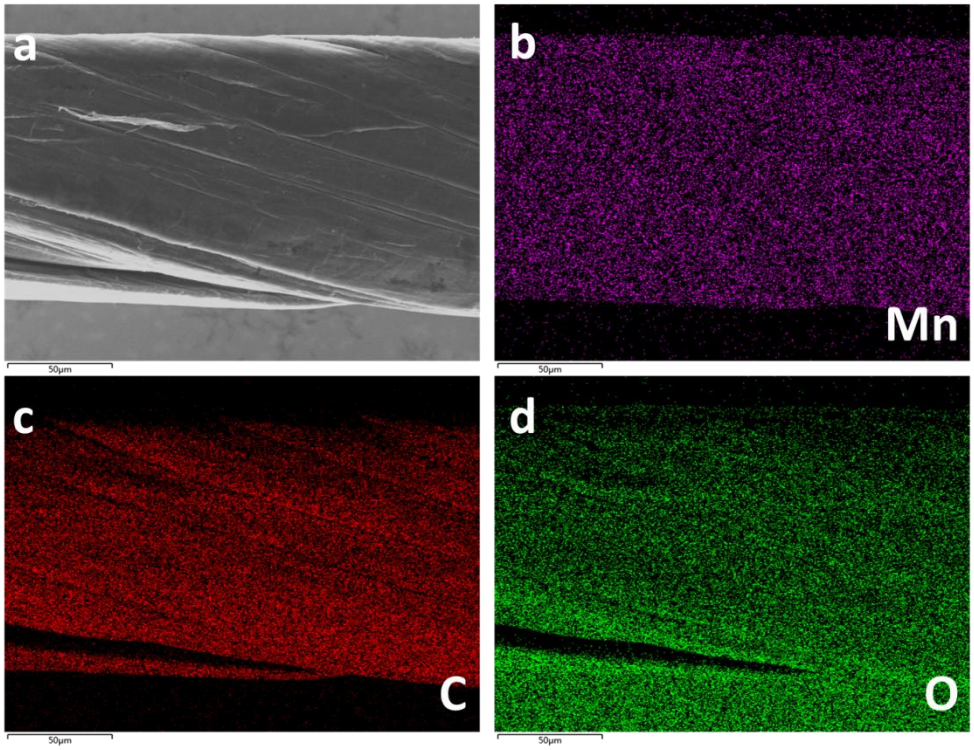

Fig. S5. (a) SEM images of MnO_2/CNT fiber with a MnO_2 growth time of 6 h. (b–d) EDS mappings of Mn, C and O element on the surface of MnO_2/CNT fiber, respectively.

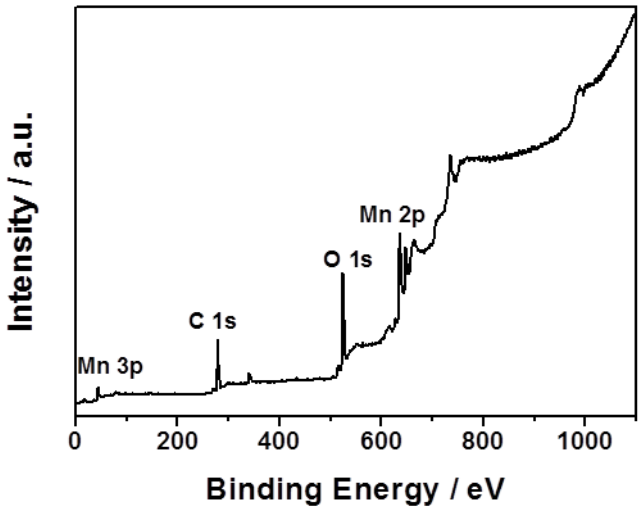

Fig. S6. XPS full spectrum of the MnO_2/CNT fiber with a MnO_2 growth time of 6 h.

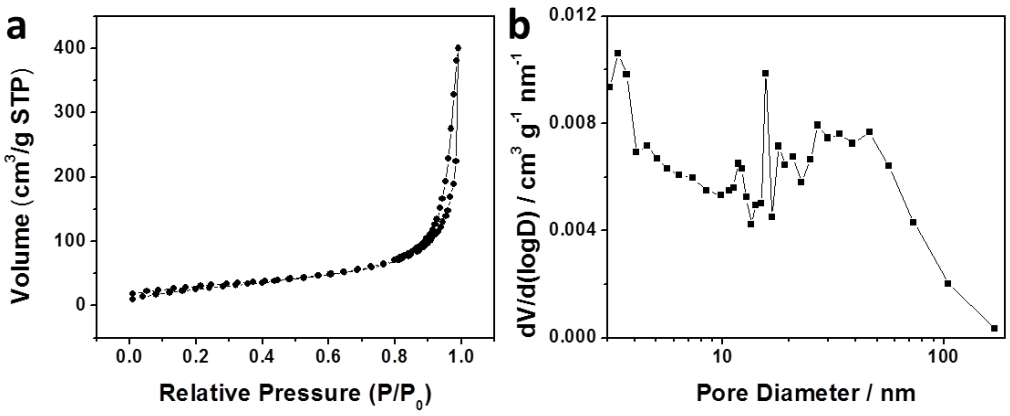

Fig. S7. (a) Nitrogen adsorption/desorption isotherm curve and (b) BJH pore size distribution of the MnO_2/CNT fiber with MnO_2 growth time of 6 h and MnO_2 weight percentage of 60.8%.

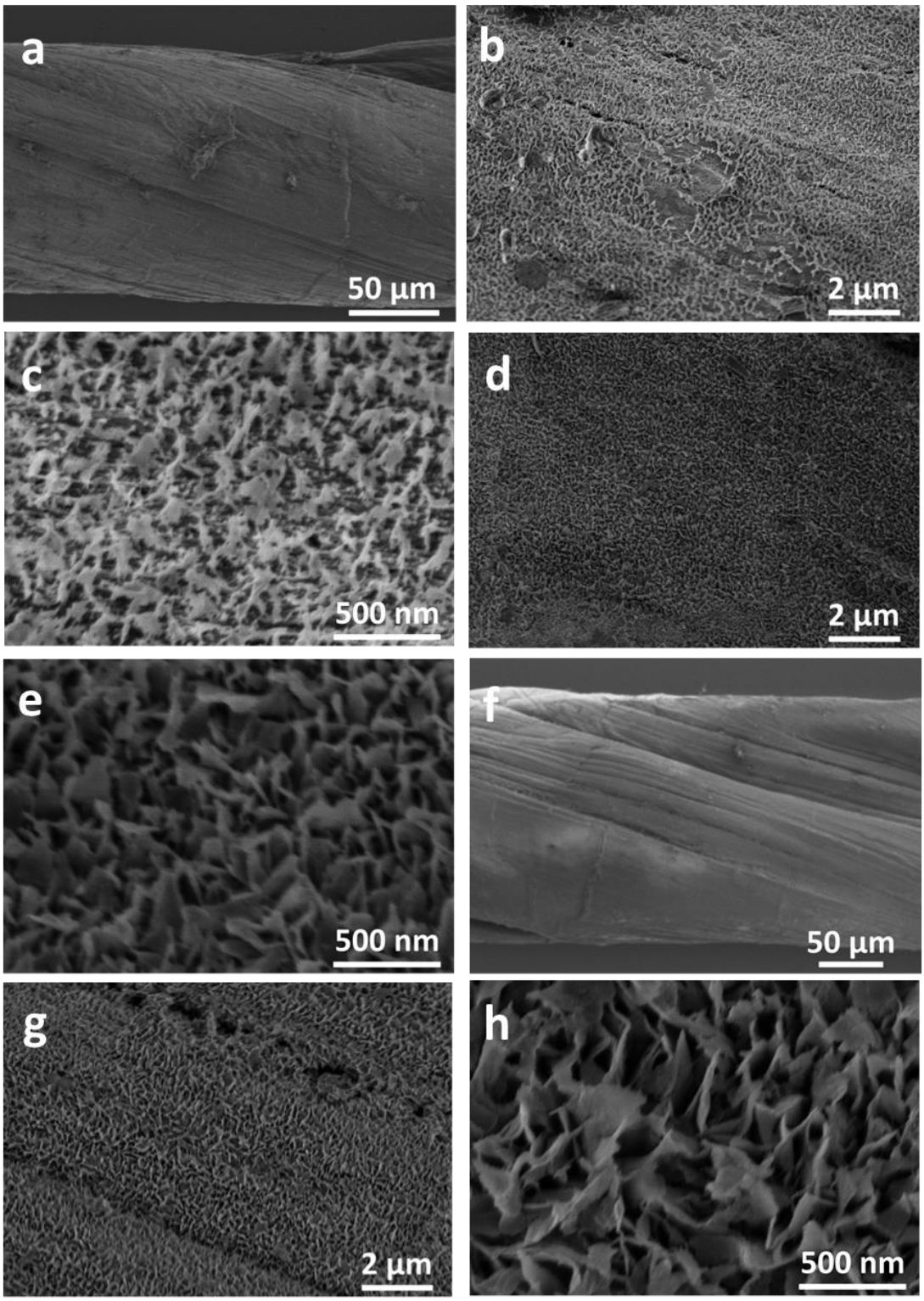

Fig. S8. SEM images of the PI/CNT fibers with PI growth time of (a-c) 3 h, (d, e) 9 h and (f-g) 12 h at different magnifications.

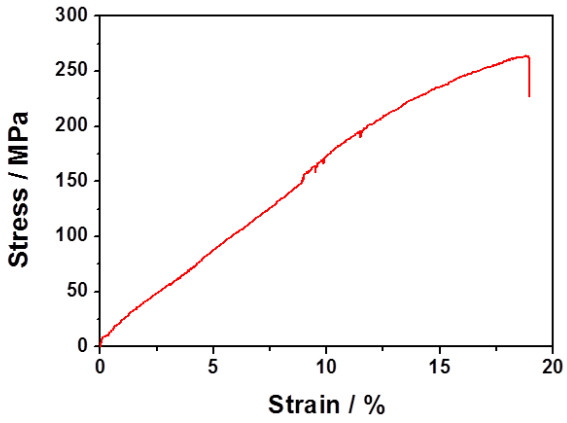

Fig. S9. Stress-strain curve of the PI/CNT fiber with a PI growth time of 9 h.

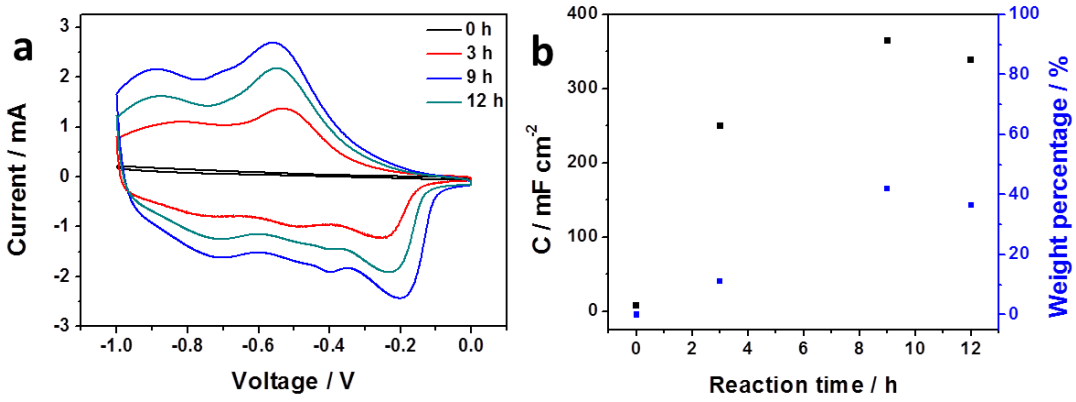

Fig. S10. (a) Comparative CV curves of PI/CNT fiber electrodes with increasing growth times at the same scan rate of 50 $mV \cdot s^{-1}$. (b) Dependence of areal specific capacitance of PI/CNT fiber and weight percentage of PI on reaction time measured at 1.76 $mA \cdot cm^{-2}$.

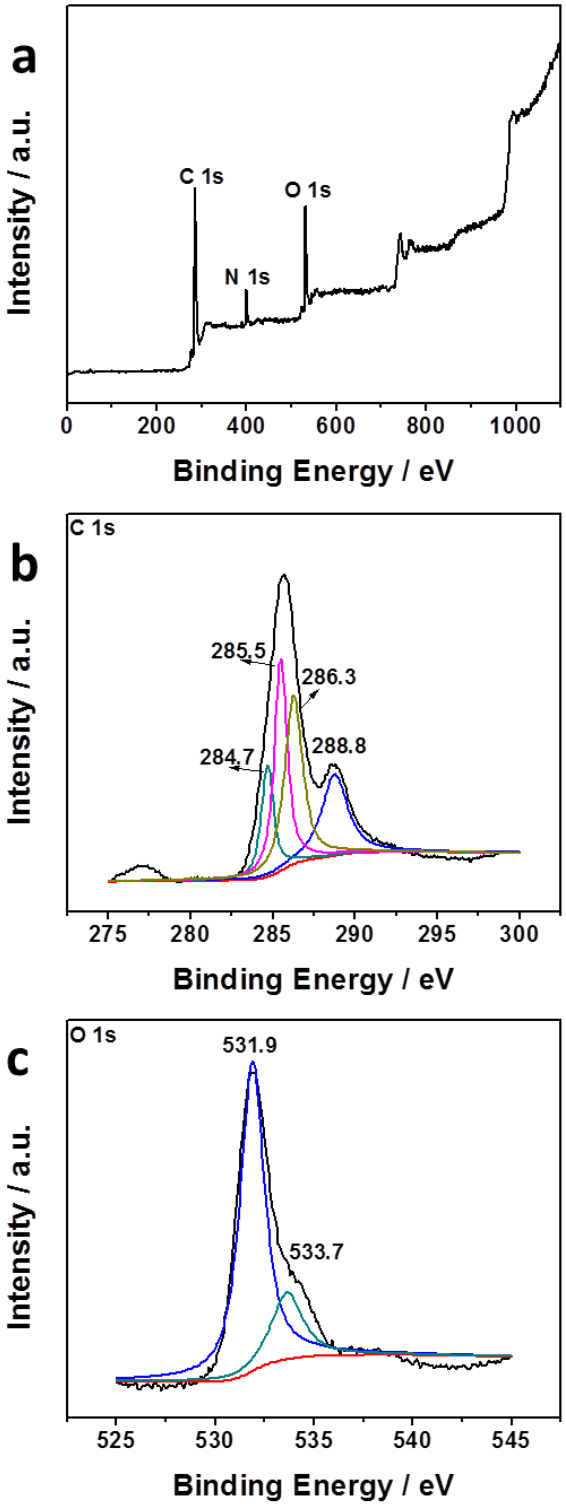

Fig. S11. XPS spectra of PI/CNT fiber with: (a) full spectrum, (b) C1s and (c) O1s.

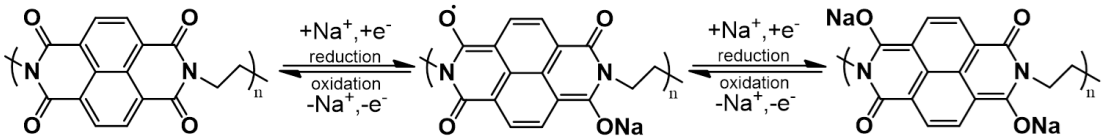

Fig. S12. The electrochemical redox reaction mechanism of PI based fiber electrode.

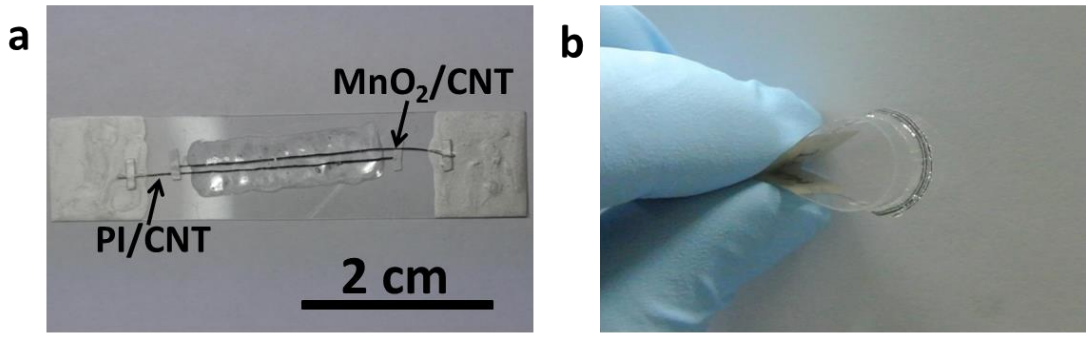

Fig. S13. (a) Photograph of a FAS on a polymer substrate. (b) Photograph of a FAS bent to 180°.

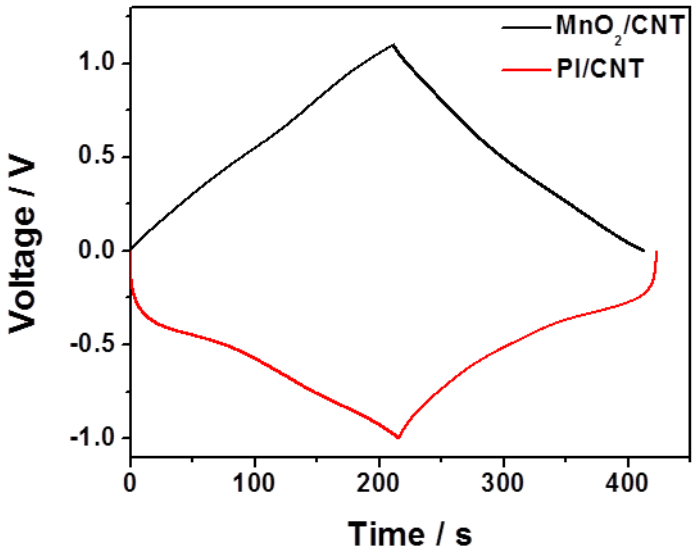

Fig. S14. Comparative charge-discharge curves of MnO_2/CNT positive and PI/CNT negative electrodes at the same current of 0.133 mA.

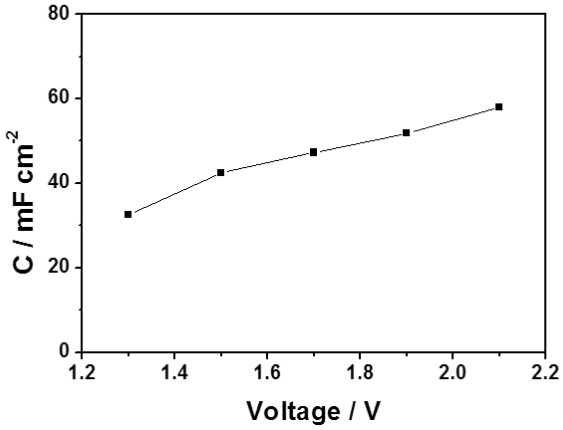

Fig. S15. Areal specific capacitance of the FAS at different voltage windows.

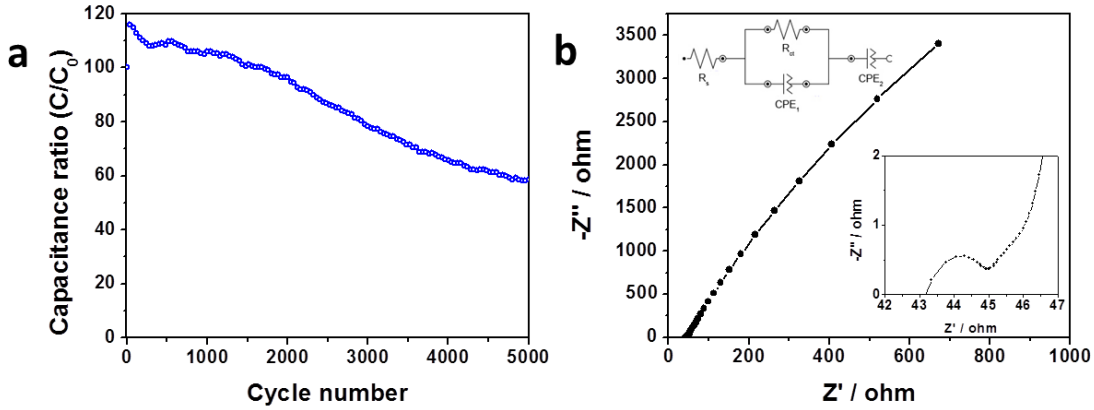

Fig. S16. (a) Plot of capacitance retention of the FAS at a current density of 14.85 mA·cm^{-2} for 5000 cycles. (b) Electrochemical impedance spectra of the FAS after 5000 charge-discharge cycles with insets showing the high-frequency parts and equivalent circuit diagram used for fitting the EIS data.

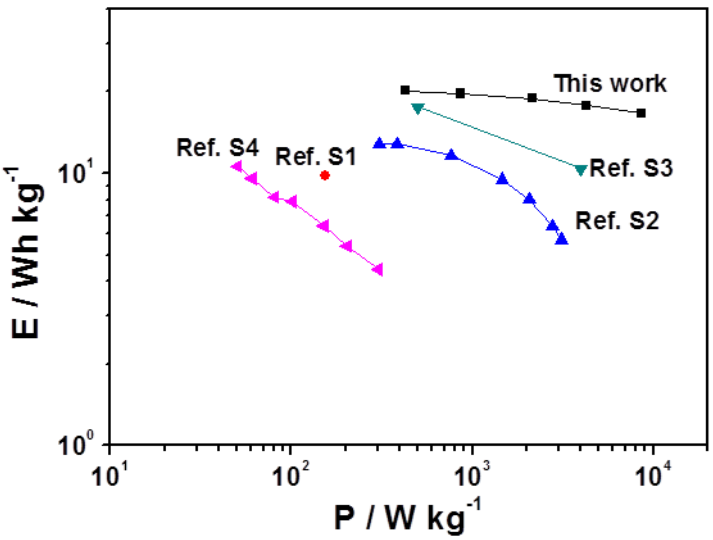

Fig. S17. Ragone plots of our FAS compared with the other reported fiber-based supercapacitors.[S1-S4]

References for the Supporting Information

S1. S. T. Senthilkumar and R. K. Selvan, *Phys. Chem. Chem. Phys.*, **2014**, 16, 15692-15698.

S2. X. Zhao, B. Zheng, T. Huang and C. Gao, *Nanoscale*, **2015**, *7*, 9399-9404.

S3. W. Xiong, X. Hu, X. Wu, Y. Zeng, B. Wang, G. He and Z. Zhu, *J. Mater. Chem. A*, **2015**, *3*, 17209-17216.

S4. S. T. Senthilkumar, J. Kim, Y. Wang, H. Huang and Y. Kim, *J. Mater. Chem. A*, **2016**, *4*, 4913-4940.